

# Phase Crossover induced by Dynamical Many Body Localization in Periodically Driven Long-Range Spin Systems

Mahbub Rahaman,<sup>1</sup> Takashi Mori,<sup>2</sup> and Analabha Roy<sup>1</sup>

<sup>1</sup>Department of Physics, The University of Burdwan, Golapbag, Bardhaman - 713 104, India

<sup>2</sup>RIKEN CEMS, 2-1 Hirosawa, Wako, Saitama, 351-0198, Japan

Dynamical many-body freezing occurs in periodic transverse field-driven integrable quantum spin systems. Under resonance conditions, quantum dynamics causes practically infinite hysteresis in the drive response, maintaining its starting value. We extended this to non-integrable many body systems by reducing the Hamiltonian symmetries through a power-law dependence in spin exchange energy,  $J_{ij} = 1/|i - j|^\beta$ . The dynamics of the integrable short-range Transverse Field Ising Model (TFIM) and non-integrable long-range Lipkin Meshkov-Glick (LMG) models were investigated. In the LMG, the resonance conditions in the driving field suppresses the heating postulated by the *Eigenstate Thermalization Hypothesis* (ETH) by inducing *Dynamical Many Body Localization*, or DMBL. This is in contrast to Many Body Localization (MBL), which requires disorder to suppress ETH. DMBL has been validated by the Inverse Participation Ratio (IPR) of the quasi-stationary Floquet modes. While TFIM has IPR localization for all drive parameters, the LMG exhibits high-frequency localization only at the resonances. IPR localization in the LMG deteriorates with an inverse system size law at lower frequencies, which indicates heating to infinite temperature. Furthermore, adiabatically increasing frequency and amplitude from low values raises the Floquet state IPR in the LMG from nearly zero to unity, indicating a phase crossover. This occurrence enables a future technique to construct an MBL engine in clean systems that can be cycled by adjusting drive parameters only.

Keywords: Dynamical localization, Thermalization, Phase Crossover

Periodically driven Quantum Many Body Systems can, under certain conditions, experience Dynamical Freezing (DMF) when dynamical hysteresis stops observables from reaching their diagonal averaged values and thermalizing to infinite temperature [1–3]. Under certain resonance conditions in the drive parameters, DMF can cause the response to ‘freeze’ completely to its initial value at all times. This arises as a consequence of additional approximate symmetries that occur at resonance. DMF has been demonstrated via the Rotating Wave Approximation (RWA) in the driven TFIM with nearest-neighbour interactions [4] and is shown to be protected when translational invariance is explicitly broken (say, by disorder) [5, 6].

The utilization of Floquet theory simplifies the analysis of time-periodic systems. For closed quantum systems governed by the time-dependent Schrödinger equation, the *Floquet Hamiltonian* allows for a mapping of the time-dependent dynamics into the dynamics of a time-independent effective Hamiltonian, provided the system is strobed at integer multiples of the time period of the drive. The time independent eigenstates of the effective Hamiltonian correspond to quasi-stationary *Floquet Modes* of the original Hamiltonian. The temporal progression of the system comes from phase coefficients that capture the dynamics [7, 8].

Any sufficiently complex non-integrable Many Body System is expected to thermalize according to the Eigenstate Thermalization Hypothesis (ETH) despite

the fact that closed quantum dynamics preserves the memory of the initial state of the system. This arises due to the properties of the matrix elements of observables in typical states[9]. The ETH can be readily adapted to time-periodic systems using Floquet theory (the Floquet-ETH, or FETH). Nonetheless, the conditions for ETH to hold are not particularly strong, and the density matrix of the system can fail to approach one that is described by a thermal expression. In such cases, the system is said to undergo *Many Body Localization* (MBL) Thermal systems must conduct because they exchange energy and particles internally during thermalization. Thus, insulating systems can be naturally athermal; Many Body Localization is a well-studied case [10]. This phenomenon is stable against local perturbations, and constitutes an exotic state of matter with far-reaching implications in theoretical physics, as well as in practical applications[11].

The addition of disorder has been identified as a crucial component in the onset of MBL. In that case, thermalization is prevented by disorder-induced localization. Nonetheless, alternative approaches to MBL in strongly interacting disorder-free systems [12–14], inhomogeneous systems [15–18], and by inducing disorder in the emergent physics [19] and by other effective means [17] (albeit with strong finite-size effects), have been reported. An alternative approach to realizing MBL in disorder-free homogeneous many-body systems involve *Floquet Engineering*, where a time-periodic drive is introduced, and the drive parameters

<sup>67</sup> tuned to introduce a clustering of quasistationary en-  
<sup>68</sup> ergies in a manner similar to localization[9].

<sup>69</sup> In this article, we propose that additional approxi-  
<sup>70</sup> mate symmetries can be Floquet-engineered in quan-  
<sup>71</sup> tum many body systems with lower symmetry than  
<sup>72</sup> the TFIM, such as those with long-range interactions.  
<sup>73</sup> This results in both DMF and MBL occurring simul-  
<sup>74</sup> taneously at resonant values of the drive parameters,  
<sup>75</sup> and complete thermal behaviour at other values. This  
<sup>76</sup> phenomenon is distinct from DMF in the TFIM, since  
<sup>77</sup> clean TFIM systems, being integrable, never thermal-  
<sup>78</sup> ize.

<sup>79</sup> To demonstrate the onset of MBL, we investigate  
<sup>80</sup> the driven Lipkin-Meshkov-Glick (LMG) model[20–  
<sup>81</sup> 25], a long-range system that is a special case of the  
<sup>82</sup> more general Curie-Weiss model, wherein the nearest-  
<sup>83</sup> neighbour exchange in the TFIM is extended to longer  
<sup>84</sup> ranges with a power law dependence,  $J_{ij} \sim 1/|i - j|^\beta$   
<sup>85</sup> [26–28]. Setting  $\beta = \infty$  recovers the TFIM, and set-  
<sup>86</sup> ting  $\beta = 0$  yields the LMG model. We have recovered  
<sup>87</sup> the onset of DMF in this system and have supported  
<sup>88</sup> our result with numerical simulations.

<sup>89</sup> In addition, we compare the degree of localization  
<sup>90</sup> of the quasi-stationary Floquet modes in both limits of  
<sup>91</sup>  $\beta$ . In order to do so, we look at the Inverse Partici-  
<sup>92</sup> pation Ratio (IPR) of the Floquet modes in the repre-  
<sup>93</sup> sentation given by the eigenstates of the symmetry-  
<sup>94</sup> breaking field. The IPR, closely related to the concept  
<sup>95</sup> of quantum purity, is defined as the formal sum of the  
<sup>96</sup> square of the density in some physically meaningful  
<sup>97</sup> space or representation. A high IPR of a stationary  
<sup>98</sup> state denotes low participation in most of the repre-  
<sup>99</sup> sentation, and a low IPR distributes participation uni-  
<sup>100</sup> formly across the representation, leading to ergodic  
<sup>101</sup> dynamics[29]. Thus, IPR [30] is a useful tool for wit-  
<sup>102</sup> nessing MBL of a quantum system. For an MBL sys-  
<sup>103</sup> tem, the IPR is unity, and it scales inversely with the  
<sup>104</sup> system-size **number of spins** when it is thermally dis-  
<sup>105</sup> tributed [31].

<sup>106</sup> In the first section of this paper, we present all es-  
<sup>107</sup> sential theoretical frameworks. Our results for the  
<sup>108</sup> LMG model are presented next in section II. In that  
<sup>109</sup> section, we have used the Rotating Wave Approx-  
<sup>110</sup> imation (RWA) [32], where only the slowest rotating  
<sup>111</sup> terms in the Fourier expansion of the Hamiltonian in  
<sup>112</sup> a frame co-rotating with the symmetry breaking drive  
<sup>113</sup> field are retained. In addition, we have the obtained  
<sup>114</sup> analytical expressions for numerical simulations of the  
<sup>115</sup> Floquet modes and their IPR. They are used to probe  
<sup>116</sup> the system dynamics in the high and low-frequency  
<sup>117</sup> domains at both limits of  $\beta$ . In section III we have  
<sup>118</sup> used phase space plots to contrast the low and high  
<sup>119</sup> frequency limits of the LMG model in the thermody-  
<sup>120</sup> namic limit by mapping it to an equivalent classical  
<sup>121</sup> Hamiltonian system. Finally, in section IV, we have

<sup>122</sup> looked at numerical computations of the IPR of the  
<sup>123</sup> Floquet modes for different values of the drive pa-  
<sup>124</sup> rameters, well beyond those that allow for the RWA.  
<sup>125</sup> We observed that, if the system is driven by an adia-  
<sup>126</sup> batically increasing drive frequency from low to high  
<sup>127</sup> limit while remaining in the resonance region, a sharp  
<sup>128</sup> crossover from a thermal to an MBL phase occurs. We  
<sup>129</sup> conclude with discussions and outlook.

## I. BACKGROUND

<sup>131</sup> The Eigenstate Thermalization Hypothesis (ETH) is  
<sup>132</sup> a series of conjectures that allows for the thermaliza-  
<sup>133</sup> tion of an isolated quantum many body system. The  
<sup>134</sup> state of the system,  $|\psi(t)\rangle$ , evolves according to the  
<sup>135</sup> Schrödinger equation  $\hat{H}|\psi(t)\rangle = i\frac{\partial}{\partial t}|\psi\rangle$ . The Hamilto-  
<sup>136</sup> nian  $\hat{H}$  is assumed to be *non-integrable*, in that it lacks  
<sup>137</sup> an extensive number of *local* additive conserved quan-  
<sup>138</sup> tities, that is to say, there are no set of observables  
<sup>139</sup>  $\hat{O}_s$  such that  $\hat{H} = \sum_s \hat{O}_s$  for any extensive index  $s$ .  
<sup>140</sup> Here, the  $\hat{O}_s$  constitute an arbitrary CSCC (complete  
<sup>141</sup> set of commuting observables) that are *local*, having  
<sup>142</sup> sub-extensive support in the system size. In addition,  
<sup>143</sup> we postulate the existence of an equivalent Hamilto-  
<sup>144</sup> nian  $\hat{H}_{eq}$  for every Hamiltonian  $\hat{H}$  as well as an "equi-  
<sup>145</sup> librium" value  $A_{eq}$  for every observable  $\hat{A}$ , such that

$$A_{eq}(E) \equiv \frac{\text{Tr}(\hat{A}e^{-\beta\hat{H}_{eq}})}{\text{Tr}(e^{-\beta\hat{H}_{eq}})}, \quad (1)$$

<sup>146</sup> where  $E = \langle\psi(t)|\hat{H}|\psi(t)\rangle$  is the conserved energy of  
<sup>147</sup> the system, and  $\beta = 1/(k_B T)$  is the inverse tempera-  
<sup>148</sup> ture,  $H_{eq}$  is an effective Hamiltonian that captures the  
<sup>149</sup> long-time average dynamics of the system, and  $k_B$  is  
<sup>150</sup> the Boltzmann constant.

To put it simply, ETH proposes that this many-body Hamiltonian undergoes thermalization as seen in the *long-time averages* of observables, with the eigenstates bearing resemblance to thermal states. The aforementioned hypothesis serves as a valuable instrument for comprehending the conduct of simulated quantum systems and their correlation with thermal equilibrium. This assertion can be justified by examining the expectation value of an observable  $\hat{A}$  as it evolves under the Schrödinger equation. To see this, we first expand the state of the system  $|\psi(t)\rangle$  as:

$$|\psi(t)\rangle = \sum_m c_m(t) |m(0)\rangle,$$

<sup>151</sup> where  $|m(0)\rangle$  represents the eigenstates of  $\hat{H}(0)$  with  
<sup>152</sup> energy  $E_m$ . The coefficients  $c_m(t)$  describe the time-  
<sup>153</sup> dependent amplitude of the expansion. Plugging

<sup>154</sup> these expansions into the expression for the expectation value, we obtain the long-time average of the <sup>155</sup> expectation value [33]:

$$\overline{\langle \hat{A}(t) \rangle} = \sum_{m,k} \overline{c_m^*(t)c_k(t)} \langle m(0)|\hat{A}|k(0) \rangle, \quad (2)$$

<sup>157</sup> where the overline indicates the following operation <sup>158</sup> for any time-dependent quantity  $\mathcal{O}(t)$ ,

$$\overline{\mathcal{O}} \equiv \lim_{t \rightarrow \infty} \frac{1}{t} \int_0^t d\tau \mathcal{O}(\tau). \quad (3)$$

Had the system been integrable, the large number of conserved quantities would restrict mixing between the states during unitary evolution. In the non-integrable case, the system explores the entire Hilbert space spanned by eigenstates with eigenvalues close to  $E$  more-or-less uniformly. In that case, the matrix elements  $\langle m(0)|\hat{A}|k(0) \rangle$  are said to satisfy the Srednicki ansatz [34, 35]:

$$\begin{aligned} \langle m(0)|\hat{A}|k(0) \rangle &\approx A_{eq} \left( \frac{E_m + E_k}{2} \right) \delta_{mk} + \\ &e^{-\frac{1}{2}S\left(\frac{E_m+E_k}{2}\right)} f \left( \frac{E_m + E_k}{2}, E_m - E_k \right) R_{mk}. \end{aligned} \quad (4)$$

Here,  $S$  is the thermodynamic entropy and  $R_{mk}$  are elements of a random matrix with vanishing mean and unit variance. What this means for the ensuing dynamics is that the system explores the accessible Hilbert space uniformly, and the matrix elements  $\langle m(0)|\hat{A}(t)|k(0) \rangle$  become indistinguishable for most pairs of  $m$  and  $k$ . Applying this ansatz and taking the thermodynamic limit by ignoring terms  $\mathcal{O}(e^{-S/2})$ , the expression for the expectation value becomes:

$$\begin{aligned} \overline{\langle \hat{A}(t) \rangle} &\approx \sum_m \overline{|c_m(t)|^2} A_{eq}(E_m) \\ &\approx A_{eq}(E) \sum_m \overline{|c_m(t)|^2} = A_{eq}(E), \end{aligned}$$

<sup>159</sup> where, in the last step, we utilized the fact that  $A_{eq}$  is <sup>160</sup> a smooth function, and that the states with energies <sup>161</sup> far from  $E$  have  $|c_m(t)|^2 \approx 0$ . Therefore, in the limit of <sup>162</sup> large systems the expectation value of an observable <sup>163</sup>  $\hat{A}$  is approximately equal to the thermal expectation <sup>164</sup> value  $A_{eq}$ . This is the essence of the ETH, which sug- <sup>165</sup>gests that individual eigenstates of a quantum system <sup>166</sup> can be described by statistical mechanics in the long- <sup>167</sup> time limit.

<sup>168</sup> We now generalize the ETH to non-integrable many <sup>169</sup> body systems that are closed, but not isolated. In <sup>170</sup> that case, it is possible to impart a periodic time- <sup>171</sup> dependence on the Hamiltonian while still ensuring <sup>172</sup> unitary evolution. If the time period of the drive

<sup>173</sup> is  $T$ , and the corresponding drive frequency  $\omega \equiv$  <sup>174</sup>  $2\pi/T$ , the Floquet theorem states that the solutions to <sup>175</sup> the Schrödinger equation can be written as  $|\psi(t)\rangle =$  <sup>176</sup>  $e^{-i\epsilon t/\hbar} |\phi(t)\rangle$ , where the  $|\phi(t)\rangle$  are  $T$ -periodic states <sup>177</sup> called *Floquet Modes*, the corresponding  $\epsilon \in \mathbb{R}$ , are <sup>178</sup> called *quasienergies*. Quasienergy values are not <sup>179</sup> unique, and can be made to be bounded within a Flo- <sup>180</sup> quet photon, viz. a range  $[-\omega/2, \omega/2]$  [36, 37]. As a <sup>181</sup> consequence, the unitary evolution operator can be <sup>182</sup> split into two parts as follows [38].

$$U(t) = e^{-i\hat{K}_F(t)} e^{-i\hat{H}_F t}. \quad (5)$$

<sup>183</sup> Here, the micromotion operator  $\hat{K}_F(t)$  is <sup>184</sup> time-periodic in  $T$ , with  $\hat{K}_F(0) = 0$ , and <sup>185</sup> the Floquet Hamiltonian  $\hat{H}_F = \hat{H}(t) - i \frac{\partial}{\partial t} \Big|_{t=T}$

$$\hat{H}_F = e^{i\hat{K}_F(t)} [\hat{H}(t) - i\partial_t] e^{-i\hat{K}_F(t)}. \quad \text{Thus, if the}$$

<sup>186</sup> system is strobed at integer multiples of  $T$  only, <sup>187</sup> then the unitary evolution matches that of a time <sup>188</sup> independent Hamiltonian  $H_F$ . This can capture most <sup>189</sup> of the exact dynamics at large frequencies.

<sup>190</sup> In such systems, the Floquet Eigenstate Thermaliza- <sup>191</sup> tion Hypothesis (FETH) posits that, subject to specific <sup>192</sup> conditions and in the context of a system of signifi- <sup>193</sup>cant size, the Floquet modes themselves exhibit ther- <sup>194</sup> mal state-like behavior, i.e.,  $\hat{H}_{eq} \approx \hat{H}_F$  in eqn 1. How- <sup>195</sup> ever, in contrast to the isolated systems, the loss of <sup>196</sup> energy conservation allows for the mixing of all Flo- <sup>197</sup> quet modes in the ensuing dynamics, not just those <sup>198</sup> with quasienergies near  $E$ . Were this to actually hap- <sup>199</sup>pen in the ensuing dynamics, it can be reconciled with <sup>200</sup> ETH [39] by ensuring that  $\beta = 0$  in eq 1. It can be rec- <sup>201</sup>onciled with ETH by ensuring that the RHS of eqn 1 is <sup>202</sup> independent of  $\beta$ , i.e., an infinite temperature ensem- <sup>203</sup>ble [39]. In other words, the nonequilibrium steady <sup>204</sup> state of the system tends to an infinite temperature, <sup>205</sup> maximum entropy density matrix.

<sup>206</sup> However, drive parameters like amplitude, fre- <sup>207</sup>quency, and duty-cycle strongly affect the structure <sup>208</sup>of the Floquet modes  $|\phi\rangle$ . Thus, they can be engi- <sup>209</sup>neered to prevent the kind of full mixing that would <sup>210</sup>lead to infinite temperatures, manifesting suppres- <sup>211</sup>sion of thermalization dynamically. Thus, this type <sup>212</sup>of *Floquet Engineering* can produce *Dynamical Many* <sup>213</sup>*Body Localization* (DMLB), where the system fails <sup>214</sup>to reach thermal equilibrium and remains localized, <sup>215</sup>possibly near its initial state, even at large times. <sup>216</sup>This paradigm seems similar to standard Many-Body <sup>217</sup>Localization [40, 41], where disorder, locality, and in- <sup>218</sup>tegrability can cause athermalism via breakdown in the <sup>219</sup>Srednicki ansatz. However, DMLB is a purely dynami- <sup>220</sup>cal phenomenon, and thus can occur regardless of dis- <sup>221</sup>order, locality of observables, or system integrability, <sup>222</sup>all of which have been studied for MBL onset [42–44].

Integrable Many Body systems do not exhibit thermalization. When subjected to time-periodic drives, Floquet engineering allows for the introduction of additional approximate conserved quantities that dynamically suppress the evolution of certain observables by hysteresis. This type of *freezing* of response has been shown in integrable systems [6]. A paradigmatic example is the driven Transverse Field Ising model (TFIM) in one dimension [45]. The Hamiltonian is given by

$$\hat{H}(t) = \hat{H}_0 + h_z(t) \hat{H}_1, \quad (6)$$

$$\hat{H}_0 = -\frac{1}{2} \sum_{i=1}^N \sigma_i^x \sigma_{i+1}^x, \quad (7)$$

$$\hat{H}_1 = -\frac{1}{2} \sum_{i=1}^N \sigma_i^z. \quad (8)$$

Here, the undriven Hamiltonian  $\hat{H}_0$  consists of nearest-neighbour interactions between  $N$  number of spin-1/2 particles on a one-dimensional spin network. The transverse field is denoted by  $\hat{H}_1$ , and is being varied by a time-periodic and harmonic signal  $h_z(t) = h_0 + h \cos \omega t$ , yielding a time period  $T = 2\pi/\omega$  with amplitude  $h$ , drive frequency  $\omega$ , and d.c. field  $h_0$ . This Hamiltonian can be readily transformed into a spinless pseudo-fermionic system via the Jordan-Wigner transformation [4]. When written in momentum space spanned by spinors  $\psi_k = (c_{-k}, c_k^\dagger)^T$  of fermions at momentum  $k$  created (annihilated) by operators  $c_k^\dagger$  ( $c_k$ ), the effective Hamiltonian

$$H(t) = \sum_{(k,-k)-\text{pairs}} \psi_k^\dagger \left[ \left( f_k - h_z(t) \right) \tau_z + \tau_x \Delta_k \right] \psi_k, \quad (9)$$

where  $f_k = \cos k$ ,  $\Delta_k = \sin k$ ,  $\tau_{xyz}$  are the three Pauli Matrices, and the sum is over distinct  $(k, -k)$  Cooper Pairs. We can transform our system to a frame that rotates with the time-varying symmetry-breaking field. This is achieved by the means of the unitary transformation operator

$$U(t) = \prod_k U_k(t) \quad (10)$$

$$U_k(t) = \exp \left\{ \left[ \frac{i\hbar}{\omega} \sin \omega t \right] \tau_z \right\}.$$

The resulting transformed Hamiltonian  $H'(t) = U^\dagger(t) H(t) U(t) - iU^\dagger(t) \partial_t U(t)$  simplifies to

$$H'(t) = \sum_{(k,-k)-\text{pairs}} \psi_k^\dagger \left[ \tau_z f_k + \tau_x \cos(\eta \sin \omega t) + \tau_y \sin(\eta \sin \omega t) \right] \psi_k, \quad (11)$$

where we defined  $\eta = 2\hbar/\omega$ . Using the Jacobi-Anger formula [46]

$$e^{i\eta \sin \omega t} = \sum_{n=-\infty}^{\infty} J_n(\eta) e^{in\omega t}, \quad (12)$$

where  $J_n(\eta)$  are Bessel Functions, the transformed Hamiltonian simplifies to

$$H'(t) = \sum_{(k,-k)-\text{pairs}} \psi_k^\dagger \left\{ \tau_z f_k + 2\tau_x \Delta_k \sum_{n \geq 0} J_{2n}(\eta) \cos(2n\omega t) - 2\tau_y \Delta_k \sum_{n \geq 0} J_{2n+1}(\eta) \sin[(2n+1)\omega t] \right\} \psi_k. \quad (13)$$

In the frequency regime  $\omega \gg f_k$ , the long-time average  $H^{RWA} \equiv \lim_{n \rightarrow \infty} \frac{1}{nT} \int_0^{nT} dt H'(t)$  can serve as a suitable approximation for  $H'(t)$ . This approximation, known as the *Rotated Wave Approximation* (RWA), eliminates the oscillating modes and results in an effective Hamiltonian that is independent of time,

$$H^{RWA} = \sum_{(k,-k)-\text{pairs}} \psi_k^\dagger \left[ f_k \tau_z + 2J_0(\eta) \Delta_k \tau_x \right] \psi_k. \quad (14)$$

It is evident that by manipulating the drive parameters, specifically the amplitude denoted by  $h$  and the frequency denoted by  $\omega$ , in a manner such that  $\eta$  is positioned on a root of  $J_0(\eta)$ , the fermion number can be conserved to a significant extent at this particular resonance. Consequently, it is feasible to exercise direct control over  $H^{RWA}$ , resulting in a comprehensive suppression of the dynamics of otherwise responsive observables.

This phenomenon is highly general in nature, and can be readily adapted to non-integrable systems. In such cases, freezing has the additional effect of inducing DMBL, suppressing thermalization to infinite temperatures. Numerical quantification of localization of a specific (quasi) stationary state in a physically significant representation can be achieved through the computation of the *Inverse Participation Ratio* (IPR). In the position representation, the IPR for a state  $|\psi\rangle$  [47–50] is defined as

$$\phi_{IPR} \equiv \int d\mathbf{x} |\langle \mathbf{x} | \psi \rangle|^4.$$

This definition can be generalized to the IPR of a state  $|\phi\rangle$  in a representation given by complete orthonormal basis  $|m\rangle$  as

$$\phi_{IPR} \equiv \sum_m |\langle m | \psi \rangle|^4. \quad (15)$$

The smallest value of the IPR corresponds to a fully de-localized state,  $\psi(x) = 1/\sqrt{N}$  for a system of size  $N$  [50, 51]. Values of the IPR close to unity correspond to localized states [52]. For a periodically driven system, we look at the IPR of the quasi-stationary Floquet modes at  $t = T$ , where  $t = 2\pi/\omega$  for drive frequency  $\omega$ . In the TFIM model, equation 14 indicates that, at resonance, when  $J_0(\eta) = 0$ , the Floquet modes are approximately given by the fermionic Fock states, which have a trivially unit IPR in the representation of the eigenmodes of the transverse field  $\hat{H}_1$  in equation 6. Here, a particular Floquet mode can be decomposed into a direct product of cooper-pair states as  $|\phi\rangle = \prod_{k,-k} |\phi_k^n\rangle$ . In the RWA limit and at resonance,  $|\phi_k^n\rangle$  has values of  $|0\rangle, |k, -k\rangle$  for two values of  $n = 0, 1$  respectively. We define the reduced IPR of  $|\phi_k^n\rangle \forall k$  to be

$$\phi_{IPR}^{(n)}(k) = |\langle 0|\phi_k^n\rangle|^4 + |\langle +k, -k|\phi_k^n\rangle|^4, \quad (16)$$

where  $n = 0, 1$ . In the RWA limit and at resonance, this quantity is unity, indicating very low participation and the onset of freezing. Figure 1 shows results from numerically simulating the TFIM dynamics. The reduced IPR for a particular Floquet mode recovered by simulating the exact Schrödinger dynamics over a single time period of the drive, and plotted as a function of momentum  $k$  for different  $\eta$ 's. At resonance, when  $\eta$  lies at the root of the Bessel function  $J_0(\eta)$ , the IPR is exactly nearly unity for all momenta. Outside this resonance, the IPR is unity only for some momenta because the effective Hamiltonian is perfect diagonal at  $k \in \{-\pi, 0, \pi\}$  as can be seen in the cross-sectional plots of figure 1. As we move away from the resonance point, IPR reduces from unity. However, as the TFIM is an integrable spin model, the IPR never drops to a value that is small enough to indicate thermalization. At low frequencies, RWA fails due to the unavailability of zero off-diagonal terms in the effective transformed Hamiltonian, as well as the absence of integrability breaking terms to counteract the off diagonal terms. Consequently, the IPR remains quite high ( $\sim 0.5$ ) even at the resonance point as can be seen figure 1. At low frequency, this is valid for all momentum and parameter  $\eta$ , see figure 2.

Because the dependence of observable expectations on the eigenstates is always fairly strong for integrable systems like the TFIM, such systems will never exhibit any kind of thermal behaviour unless integrability breaking terms (such as strong disorder) are included [6]. As a result, it is not physically meaningful to refer to the unit IPR region as "Many Body Localization", because the parameter space lacks a thermalized region to contrast with this state. The type of Floquet Engineering described above, on the other hand, can be easily applied to a broad class of nonintegrable systems where FETH is expected to hold in certain re-

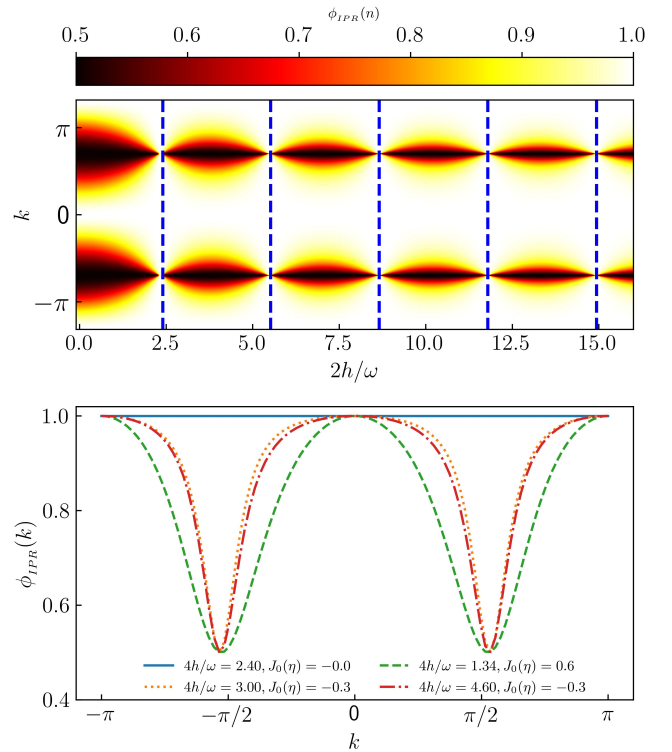


FIG. 1. Reduced IPR (defined in equation 16) for one of the two Floquet modes obtained from the exact dynamics of the TFIM for size  $N = 100$  and  $\omega = 90$  for the entire Brillouin zone (top panel, ordinate) and a few drive amplitudes (top panel, abscissa). The dashed lines (top panel) indicate the roots of  $J_0(\eta)$ . The bottom panel shows cross-sections for four different chosen amplitudes.

gions. Long-range spin systems, in particular, where the exchange energies between far-off spins are taken into account in the model Hamiltonian, are good candidates because they are known to thermalize when driven with low frequencies [53].

## II. LONG RANGE INTERACTIONS: THE LIPKIN MESHKOV GLICK MODEL:

The periodically driven Curie-Weiss Lipkin Meshkov Glick (LMG) model [20, 54] for  $N$  long-range spins is described by the Hamiltonian

$$\hat{H}(t) = \hat{H}_0 + [h \cos(\omega t) + h_0] \hat{H}_1. \quad (17)$$

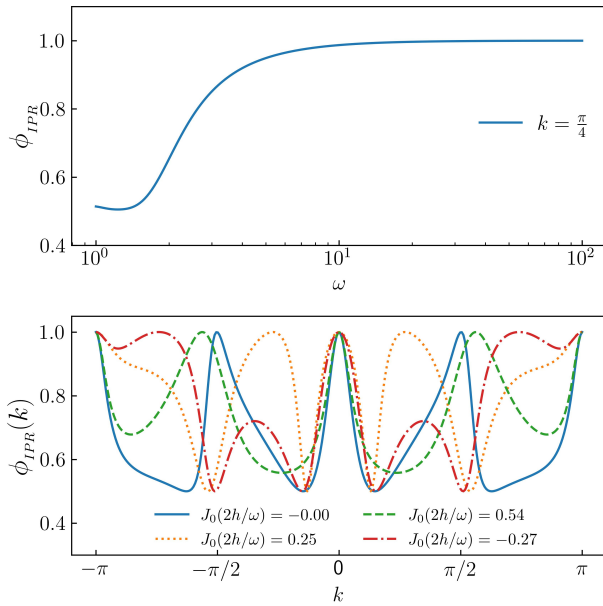


FIG. 2. Reduced IPR obtained by adiabatically increasing  $\omega$  (top panel abscissa) for one the floquet mode obtained from equation 16 at the root of  $J_0(\eta)$  for  $N = 500$ . IPR is  $\sim 0.5$  (localized yet not fully freezing) upto  $\omega \sim 2$ , after that, smoothly increased to unity (fully localized and freezing) at higher  $\omega \geq 10$  (top panel, ordinate). At bottom panel cross-sections for four chosen amplitudes at  $\omega = 2$  are plotted for a brillouin zone (abscissa) with corresponding reduced IPRs (ordinate).

<sup>321</sup> Here, the undriven part  $\hat{H}_0$  and the driven part  $\hat{H}_1$  are,  
<sup>322</sup> respectively,

$$\begin{aligned} \hat{H}_0 &= \frac{2}{N-1} \sum_{ij} \hat{\sigma}_i^z \hat{\sigma}_j^z, \\ \hat{H}_1 &= \sum_{i=1}^N \hat{\sigma}_i^x. \end{aligned} \quad (18)$$

The Kac-norm of  $2/(N-1)$  arises from the choice to maintain the extensivity of the interaction energy. The Hamiltonian in equation 17 commutes with  $P_{ij} \equiv \frac{1}{2}(1 + \vec{\sigma}_i \cdot \vec{\sigma}_j)$ . In addition, it also commutes with the total angular momentum  $S^2 = |\vec{S}|^2$ , where  $\vec{S} = S^x \hat{x} + S^y \hat{y} + S^z \hat{z} \equiv \frac{1}{2} \sum_i \vec{\sigma}_i$ . We now choose to pop-

ulate the system in a state with  $S^2 = \frac{N}{2} \left( \frac{N}{2} + 1 \right)$ . In that case, the dynamics remains invariant in the  $N+1$ -dimensional space spanned by the common eigenstates of  $P_{ij}, |S|^2$  and  $S_z$ ; the so-called *Totally Symmetric Subspace*, or TSS [55]. Let the eigenvalues of  $S^z$  in the TSS be  $s_n$ , and the eigenvectors be  $|s_n\rangle$ . Here,  $s_n = -\frac{1}{2} + \frac{n}{N}$  and the index  $n = 0(1)N$  has  $N+1$  values. The dynamics is restricted to this invariant subspace, wherein the matrix elements of the Hamiltonian are given by

$$\begin{aligned} \langle s_i | \hat{H}_0 | s_j \rangle &= -\frac{4}{N-1} s_i^2 \delta_{ij}, \\ \langle s_i | \hat{H}_1 | s_j \rangle &= \left[ \sqrt{\frac{N}{2} \left( \frac{N}{2} + 1 \right) - N s_i (N s_{i+1})} \delta_{i+1,j} \right. \\ &\quad \left. + \sqrt{\frac{N}{2} \left( \frac{N}{2} + 1 \right) - N s_i (N s_{i-1})} \delta_{i-1,j} \right]. \end{aligned} \quad (19)$$

<sup>323</sup> These allow for a numerical representation of the  
<sup>324</sup> Hamiltonian in the TSS.

<sup>325</sup> Next, we transform the Hamiltonian to the rotated  
<sup>326</sup> frame given by the operator

$$\hat{U}(t) = \exp \left[ i \frac{\hbar}{\omega} \sin(\omega t) \hat{H}_1 \right]. \quad (20)$$

<sup>327</sup> This is analogous to the rotation performed for the  
<sup>328</sup> TFIM in eqns 10 and 11. Defining  $\tau = \frac{\hbar}{\omega} \sin \omega t$ , we use  
<sup>329</sup> the fact that  $\hat{H}_1 = 2S^x$ , as well as the following iden-  
<sup>330</sup> tity obtained by using the Baker-Campbell-Hausdorff  
<sup>331</sup> formula,

$$e^{i2\tau \hat{S}^x} \hat{S}^z e^{-i2\tau \hat{S}^x} = \hat{S}^z \cos(2\tau) + \hat{S}^y \sin(2\tau), \quad (21)$$

to simplify the transformed Hamiltonian  $\tilde{H}(t) = \hat{U}^\dagger(t) \hat{H}(t) \hat{U}(t) - \hat{U}^\dagger(t) \partial_t \hat{U}(t)$ , yielding

$$\begin{aligned} \tilde{H}(t) &= -\frac{1}{N-1} \left[ (S^z)^2 (1 + \cos 4\tau) + (S^y)^2 (1 - \cos 4\tau) \right. \\ &\quad \left. + \{S^y, S^z\} \sin 4\tau \right] - 2h_0 S^x. \end{aligned} \quad (22)$$

<sup>332</sup> Next, we define  $\eta \equiv 4h/\omega$  and use the Jacobi-Anger  
<sup>333</sup> formula in eqn 12 to expand  $\tilde{H}(t)$ . This yields

$$\tilde{H}(t) = -\frac{\hat{S}^2}{N-1} + \frac{(\hat{S}^x)^2}{N-1} - 2h_0\hat{S}^x - \frac{J_0(\eta)}{N-1} \left[ (\hat{S}^z)^2 - (\hat{S}^y)^2 \right] - \frac{2}{N-1} \left[ (\hat{S}^z)^2 - (\hat{S}^y)^2 \right] \sum_{k=1}^{\infty} J_{2k}(\eta) \cos(2k\omega t) - \frac{2}{N-1} \{ \hat{S}^y, \hat{S}^z \} \sum_{k=1}^{\infty} J_{2k-1}(\eta) \sin[(2k-1)\omega t]. \quad (23)$$

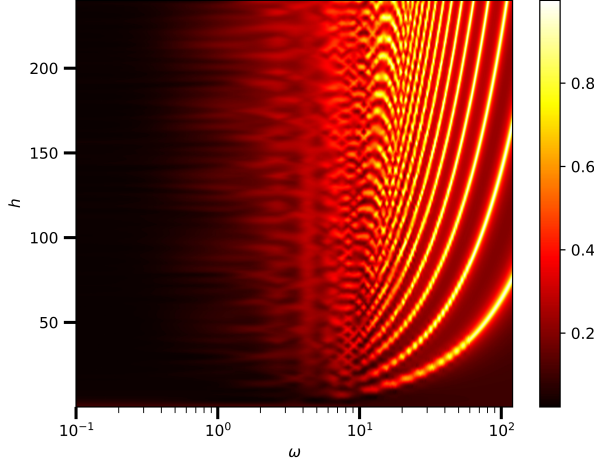


FIG. 3. Plot of the numerically averaged IPR (IPR computed using eqn 26) in the TSS plotted in the  $h - \omega$  plane for  $N = 100$  spins. In order to display the thermalized region more clearly,  $\omega$  is plotted on a logarithmic scale on the abscissa. Note that, since the IPR is clearly non-negative, an average IPR of zero means that all Floquet states have zero IPR. Furthermore, the boundedness of IPR in  $\phi_{IPR}(n) \leq 1$  ensures that if the average IPR is unity, then all Floquet states have unit IPR.

If  $\omega$  is large enough to smooth out the harmonic components, we obtain the RWA,

$$\tilde{H}(t) \approx \tilde{H}_{\text{RWA}} \equiv -\frac{\hat{S}^2}{N-1} + \frac{(\hat{S}^x)^2}{N-1} - 2h_0\hat{S}^x - \frac{J_0(\eta)}{N-1} \left[ (\hat{S}^z)^2 - (\hat{S}^y)^2 \right]. \quad (24)$$

If the drive amplitude  $h$  is adjusted such that  $\eta$  lies at a root of  $J_0(\eta)$  (the localization point), the RWA Hamiltonian is diagonal in the representation of the simultaneous eigenstates of transverse field  $\hat{S}^x$ , and  $S^2$ , yielding an IPR of unity in that representation, similar to the TFIM in the previous section. Note however, that if the DC transverse field  $h_0$  is set to 0, then, at the localization point, the RWA Hamiltonian  $\tilde{H}_{\text{RWA}} \sim (\hat{S}^x)^2$  in the TSS. The eigenvalues are two-fold degenerate. This produces infinitely many (Floquet) eigenmodes in the degenerate subspace whose IPRs may not always

be unity in the  $S^x$  representation. The removal of this degeneracy necessitates the inclusion of the d.c. field  $h_0$ . However, note that rational values of  $h_0$  may add accidental degeneracies in  $\tilde{H}_{\text{RWA}}$ . To see this, note that, at a localization point, the eigenvalues of  $\tilde{H}_{\text{RWA}}$  in the TSS are given by

$$\text{Eigs}[\tilde{H}_{\text{RWA}}] = \frac{\left(\frac{N}{2} - m\right)^2}{N-1} - 2h_0 \left(\frac{N}{2} - m\right), \quad (25)$$

where the half-integer  $-N/2 \leq m \leq N/2$  is the eigenvalue corresponding to a particular eigenstate  $|m\rangle$  of the symmetry-breaking field  $\hat{S}^x$ . In order to ensure that no additional degeneracies occur, we have to set  $h_0$  in such a way that no two energies accidentally coincide. If  $N \gg 1$  (substantially large), then this condition can be readily met by assuring that  $(1 - 2h_0)^{-1}$  is never an integer that is divisible by  $N$ . To ensure this in our numerical simulations, we have kept  $h_0$  at a small irrational value. The localization of the Floquet states at resonance is supported by exact numerical results, as can be seen in the phase diagram fig 3. Here, we have plotted the arithmetic mean over all Floquet states of the IPR in the TSS for each point in the  $h - \omega$  plane for  $N = 100$  spins. The IPR in  $S^x$  representation is

$$\phi_{IPR}(n) = \sum_m |\langle m | \phi^n \rangle|^4. \quad (26)$$

As can be readily seen in the figure, the IPR is essentially zero when  $\omega \lesssim 1$ . There is considerable structure in the phase diagram for larger drive frequencies, and along the lines given by the roots of  $J_0(\eta)$ , the IPR is essentially unity, in agreement with eqn. 24.

In figure 4, we show plots of the IPR of the Floquet modes  $|\phi^n\rangle$  for  $S^2 = (N/2)(N/2+1)$ . These plots were obtained numerically by diagonalizing the propagator  $U(t)$  at  $t = T$ , where  $U(t)$  is defined in eqn 5. This propagator was obtained from simulations of the exact quantum dynamics using QuTiP, the Quantum Toolbox in Python [56]. We kept the frequency at a fairly large value  $\omega = 90$  where we expect that RWA would be valid, and  $N = \mathcal{O}(10^2)$ . The density plot in the upper panel of fig 4 depicts the IPR of the Floquet states; the abscissa  $\eta = 4h/\omega$  and the ordinate is  $n/(2N+1)$ , where  $n \leq 2N$  is a non-negative integer

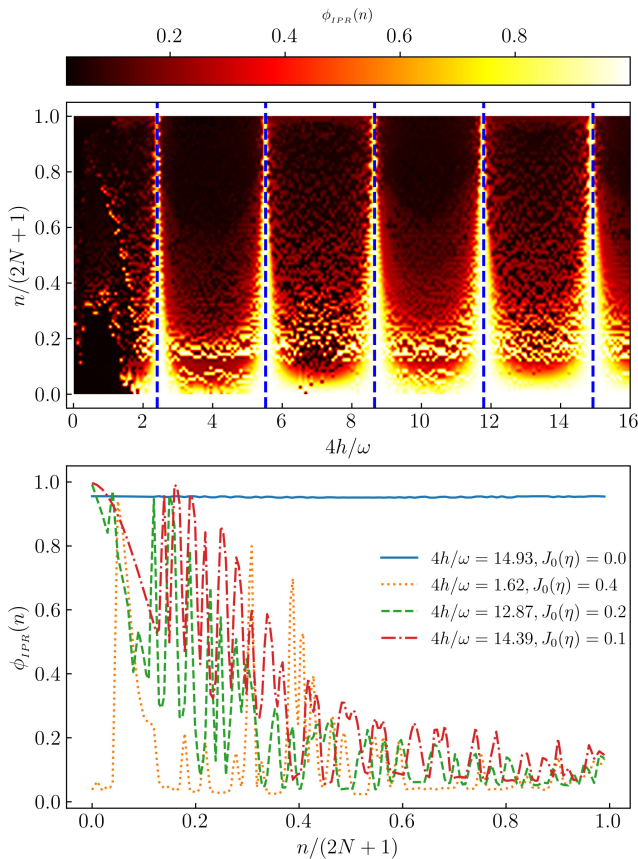


FIG. 4. IPR density plot for all possible Floquet modes (top panel ordinate) for different values of  $\eta = 4h/\omega$  (top panel abscissa), deduced from equation 26 for exact LMG Hamiltonian for  $N = 50$ . Blue dashed lines are roots of  $J_0(\eta)$ . At bottom panel cross-section of IPR (ordinate )for four different  $\eta$ 's plotted for all possible floquet modes(bottom panel, abscissa) at  $\omega = 90$ . IPR founds to be  $\sim$  unity for all Floquet modes at roots of  $J_0$ .

that indexes the Floquet states in increasing order of  $m$ . The dashed vertical lines correspond to the roots of  $J_0(\eta)$ . Comparing with the IPR of the TFIM in fig 1, we can see a very similar patterns in the immediate neighbourhood of the roots. Evidently, the IPR approaches a value of one for sufficiently large values of the roots, strongly suggesting full DMBL. Deviations occur at the smallest root of  $J_0(\eta)$  (around  $\eta = 2.405$ ) due to the contributions from higher order terms in eq 23. Thus, a higher root is favored for DMBL.

The bottom panel of fig 4 contains cross sections of the full IPR plot for selected values of  $\eta$  as indicated in the legend. When the drive amplitude  $h$  is adjusted such that  $\eta$  is close to a root of  $J_0(\eta)$ , the Floquet States are mixed, but not entirely thermal, since the IPR does not fall to  $\mathcal{O}(N^{-1})$ , indicating that localization persists to some extent. However, the further we are from the roots, the closer the IPR gets to one predicted by thermalization.

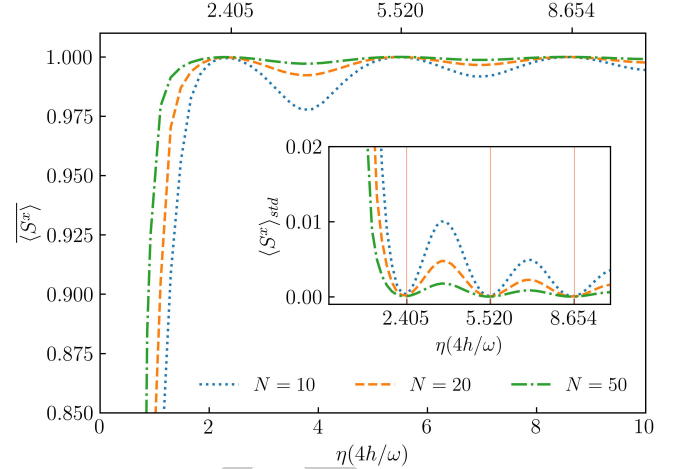


FIG. 5. Temporal average of  $\langle \hat{S}^x \rangle$  (ordinate) for different  $\eta$ 's (abscissa) is plotted for  $\sim 200T$  at higher  $\omega$  for different  $N=10, 20, 50$ .  $\langle \hat{S}^x \rangle$  is found to be unity at roots of  $J_0(\eta)$ . At points away from resonance points,  $\langle \hat{S}^x \rangle$  falls below unity. The corresponding standard deviation  $\langle \hat{S}^x \rangle_{std}$  supports the variation of  $\langle \hat{S}^x \rangle$  (inset fig.).  $\langle \hat{S}^x \rangle_{std}$  is  $\sim 0$  describing a full freezing of the system at roots of  $J_0(\eta)$  (red vertical solid lines).

Figure 5 shows plots of the long-time average (from  $t = 0 - 200T$ ) of the field amplitude  $\langle \hat{S}^x \rangle$  as a function of  $\eta$ . The system is started from the fully polarized state  $s_n = N/2$  in the TSS and the dynamics simulated. The average is plotted for different values of amplitude  $h$ , keeping the frequency fixed at a high value of  $\omega = 90$ . It is clearly very close to unity at roots of  $J_0(\eta)$  and falls at points away from it, indicating that  $S^x$  is approximately conserved at the localization points.

Small deviations do occur due to the role of higher order terms in the rotated Hamiltonian in eq 22. This can be demonstrated quantitatively by comparing the IPR obtained from the exact dynamics simulation with that obtained from the dynamics of  $\tilde{H}(t)$  in eq. 22 after truncating the series at orders  $k \geq 1$ . This comparison can be seen in fig 6. The IPR plots from the exact dynamics indicate that the first localization point, represented by the lowest root of  $J_0(\eta)$ , does not show complete DMBL. However, DMBL is particularly conspicuous at large roots. The IPRs of the Floquet states obtained from the RWA dynamics exhibit large deviations from unity when away from the localization point as evidenced by the green and red curves in the middle panel of fig 6. However, complete localization is seen in the RWA dynamics at any localization point, in contrast to the exact case in the top panel. Thus, it is necessary to incorporate higher-order corrections into the Rotating Wave Approximation (RWA) at lower

### 438 III. PERSISTENCE OF DMBL IN THE CONTINUUM 439 LIMIT

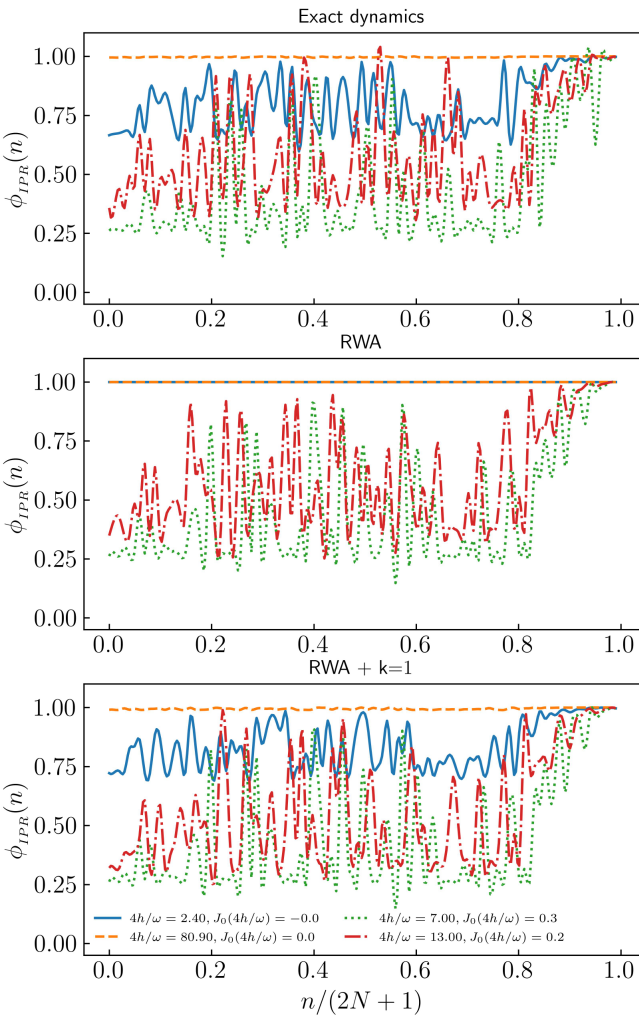


FIG. 6. The comparison between IPR for exact dynamics and RWA with corresponding correction orders. IPR is calculated for four different  $\eta$ 's and corresponding  $J_0(\eta)$  values for colors, Blue :  $\eta = 2.40$ ,  $J_0(\eta) = 0.0$ , dashed orange:  $\eta = 80.9$ ,  $J_0(\eta) = 0.0$ , Green:  $\eta = 7.0$ ,  $J_0(\eta) = 0.3$ , Red:  $\eta = 13$ ,  $J_0(\eta) = 0.2$ . At low root of  $J_0(\eta)$  IPR is not unity (Blue curve) where at higher root (orange dashed) it is unity while at points away from roots IPR are less than unity in the exact (top panel) plot. RWA does not matches with the exact plot. At all roots of  $J_0(\eta)$  IPR is unity(middle panel). RWA with additional higher order terms exhibit similar system pattern(Bottom panel) with exact dynamics.

434 localization points. The application of the first-order  
 435 correction to RWA in the lower panel of fig 6 results in  
 436 a curve structure that is closer to that from the exact  
 437 dynamics.

440 In the continuum limit, where  $N \rightarrow \infty$ , the disparity  
 441 between neighboring values of  $s_i$  in equation 19 can  
 442 be disregarded, and  $s_i$  can be mapped to a continuum  
 443  $q \in [-1/2, 1/2]$  [55]. We define the Hamiltonian per  
 444 particle  $h(t) \equiv \frac{H(t)}{N}$ , and a canonically conjugate co-  
 445 ordinate  $Np \equiv \left\langle -i \frac{\partial}{\partial q} \right\rangle$ . Then, in this limit, the dynam-  
 446 ics can be approximated by that of a classical Hamil-  
 447 tonian [57]

$$h(t) = -2q^2 - [h \cos \omega t + h_0] \sqrt{1 - 4q^2} \cos p, \quad (27)$$

which yields the dynamical system

$$\begin{aligned}\frac{dq}{dt} &= \frac{\partial h}{\partial p} = h(t) \sqrt{1 - 4q^2} \sin p \\ \frac{dp}{dt} &= -\frac{\partial h}{\partial q} = 4q \left[ 1 - \frac{h(t) \cos p}{\sqrt{1 - 4q^2}} \right],\end{aligned}\quad (28)$$

where  $h(t) = [h \cos \omega t + h_0]$ . We have profiled simulations of the ensuing dynamics with the *Poincaré surface of section* (PSOS) of the full dynamics. Here, the  $(q, p)$ -phase space is strobed at  $t = nT$ , and plotted for a large number of initial conditions. The results are shown in the upper panels of fig 7 for a small value of  $\omega = 2.0$  (left panel) and a large value  $\omega = 90$  (right panel). In both cases, the value of  $h$  is chosen such that  $\eta$  lies on the first root of  $J_0(\eta)$ . The onset of chaos for small drive frequency indicates thermal behaviour for typical initial conditions, with small islands of regularity for others. This is consistent with similar results for small frequencies reported in [53, 58]. However, at high frequency, the regular islands distinctly dominate over the chaos. The trajectories indicate that the conservation of  $\langle S^x \rangle \approx \sqrt{1 - 4q^2} \cos p$  [55] at high  $\omega$  persists in the thermodynamic limit. That this is a signature of the underlying quantum dynamics can be readily seen in the quantum phase space representation of the Floquet Eigenstates for a large but finite  $N$ . These are shown in the corresponding lower panels of fig 7. Here, we have plotted the Spectral Average of the Husimi Q-functions of the acquired Floquet States in the TSS. Specifically, for a coherent state  $|q, p\rangle$ , the corresponding Spectral-Averaged Husimi distribution [59] is obtained by

$$H(q, p) \equiv \frac{1}{(2N+1)\pi} \sum_n \langle q, p | \phi^n \rangle \langle \phi^n | q, p \rangle. \quad (29)$$

<sup>474</sup> The quantum phase space retains signatures of the  
<sup>475</sup> classical phase space dynamics when  $N = 100$ , indi-  
<sup>476</sup> cating the onset of the persistence of  $S^x$  conservation  
<sup>477</sup> that arises from the resonance condition at high fre-  
<sup>478</sup> quencies.

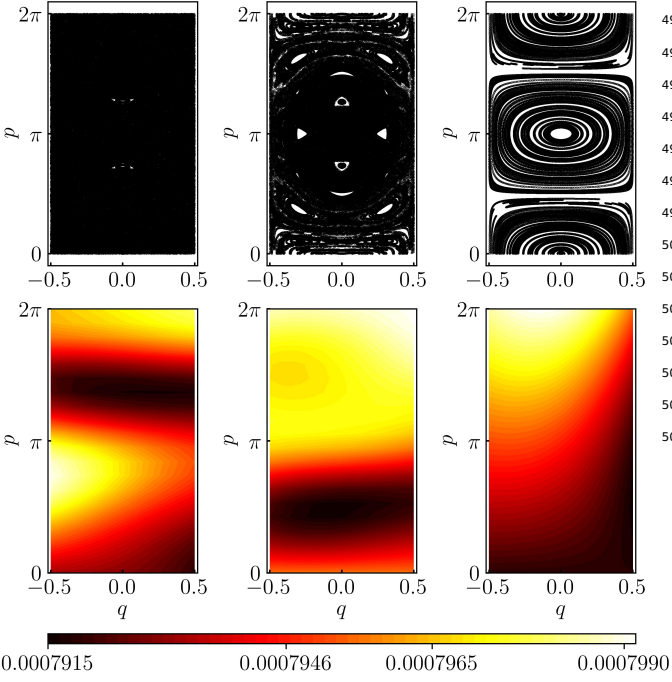


FIG. 7. Phase-space distributions at  $\omega = 1.0$  (left panels),  $\omega = 2.5$  (middle panels) and  $\omega = 90.0$  (right panels) for 100 initial conditions. The drive amplitude  $h$  is always adjusted such that  $\eta = 4h/\omega$  lies on the smallest root of  $J_0(\eta)$ , i.e.  $\eta = 2.4048\dots$ . At small  $\omega = 1.0$ , the classical PSOS, obtained from simulating the dynamics in eqns 28 (top left panel), shows chaotic behaviour, and at  $\omega = 2.5$ , regular regions start to appear. At higher  $\omega = 90.0$ , the dominance of regular dynamics can be readily seen (top right panel). The bottom panels plot the corresponding Spectral-Averaged Husimi-Q function, obtained from the Floquet modes  $|\phi^n\rangle$  using eqn. 29, and setting  $N = 100$ . The  $\omega = 1.0$  case (bottom left panel) has a dispersed distribution in colour. This is consistent with the chaotic behaviour seen in the continuum limit. At  $\omega = 2.5$  (bottom middle panel), there is a partial regular pattern observed together with a dispersed pattern. In the  $\omega = 90$ -case (bottom right panel), the distribution has distinct colour contrasts, which is consistent with the regular dynamics pattern seen in the continuum limit.

#### IV. PHASE CROSSOVER FROM THERMAL TO DMBL

The analysis of the periodically driven LMG model reveals two distinct scenarios at low and high external drive frequencies. In the former case, thermalization in accordance with FETH is seen, whereas in the latter case, DMBL is induced. As a result, we hypothesize that a macroscopic change in phase occurs due to the influence of frequency.

To demonstrate this, we investigate the IPR of the Floquet mode with smallest quasienergy for numerous frequencies and system sizes, along with the associated drive amplitude  $h$  keeping the system at a localization point. The results are shown in fig 8. In the

low-frequency range  $\omega \in [1.0, 9.0]$ , the IPR exhibits values well below unity. Moreover, the IPR gradually diminishes with increasing system size, following a system size inverse proportional trend, which confirms the participation distribution (as shown in the bottom panel). As the limit  $N \rightarrow \infty$ , the inverse participation ratio (IPR) tends towards zero, indicating a fully delocalized state. The plots reveal a gradual increase in the unity of IPR over a certain frequency range, specifically at  $\omega \approx 5$ . In addition, the rise does not cross with those for different values of  $N$ , suggesting the onset of a phase crossover [41, 60]. As the size of the system increases, the crossover region becomes smoother, rather than sharper.

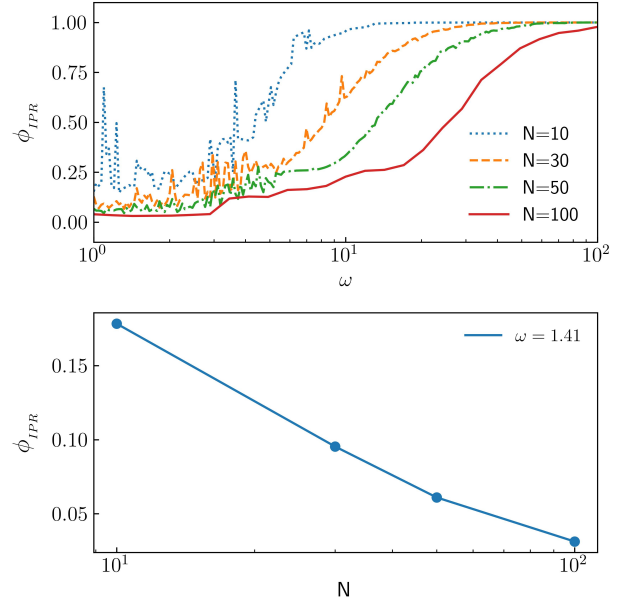


FIG. 8. IPR is plotted (top panel, ordinate) for a range of  $\omega \in [1, 100]$  (top panel, abscissa) for four different  $N = 10, 30, 50, 100$  at root of  $J_0(\eta)$ . At small  $\omega$  upto  $\omega \sim 10$  IPR founds to be very small and rises slowly upto unity (fully localized) at higher frequencies. At bottom panel IPR (ordinate) is plotted for different  $N = 10, 30, 50, 100$  (bottom panel, abscissa) for a random small  $\omega \sim 1$  at root of  $J_0(\eta)$  from the values from top panel. IPR falls as inversely proportional to  $N$ , indicating an approach to a fully distributed (thermal) state. The smooth rise in IPR defines a phase crossover (top panel) between a fully thermal phase to a fully localized phase.

We can also look at this crossover more clearly in the plots of the heating rate of the system, defined simply by the expectation value of the Hamiltonian,  $\langle \hat{H}(t) \rangle$ . We have carried out the numerical evaluation from the simulated dynamics over  $t = 500T$ . When the system is adequately described by FETH, the temporal fluctuations in the heating rate, defined

516 by  $\langle H \rangle_{std}^2 \equiv \overline{\langle \hat{H} \rangle^2} - \overline{\langle \hat{H} \rangle}^2$  (see eqn 3), are minimal in  
 517 the thermodynamic limit, as the spread of states leads  
 518 to a limited standard deviation[61]. Conversely, the  
 519 onset of athermalism is indicated by nonzero fluctua-  
 520 tions in time. If we set the initial state to the fully po-  
 521 larized state in the TSS (given by  $|s_N\rangle$ ), then the onset  
 522 of freezing, together with DMBL, will result in nearly  
 523 infinite hysteresis in the ensuing dynamics, causing  
 524  $|\psi\rangle(t) \approx |s_N\rangle \forall t$ . From eqn. 17, we can clearly see  
 525 that this will lead to a linearly rising dependence on  
 526  $\omega$  in  $\langle H \rangle_{std}$  as long as we stick to a localization point  
 527 given by a fixed  $h/\omega$  [62]. All these observations are  
 528 corroborated by the heating rate plots in figure 9.

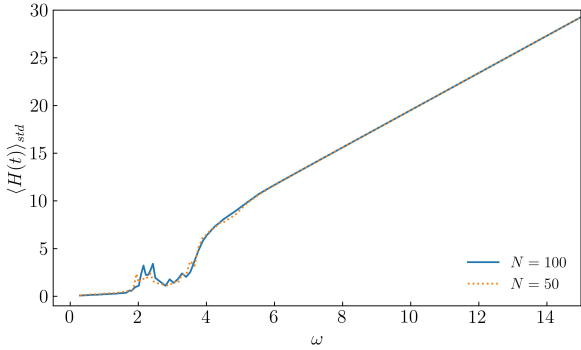


FIG. 9. The standard deviation of the heating rate, denoted by  $\langle H \rangle_{std}$ , calculated over a span of  $t = 500T$  for two system sizes. Here,  $h$  is varied to keep  $\eta = 4h/\omega$  at the first root of  $J_0(\eta)$ . A nonsingular rise has been identified at  $\omega \approx 4.0$ .  $\langle H \rangle_{std}$  exhibits a diminutive magnitude below that value of  $\omega$ , while a linear rise is observed at higher frequencies, consistent with freezing. A vanishingly small standard deviation for  $\omega \ll 4.0$  indicates the presence of a thermal region, whereas a larger finite standard deviation suggests the existence of athermal behaviour. The small peaks observed at  $\omega \in [2, 4]$  are finite-size effects that disappear in the thermodynamic limit.

529

530

## V. CONCLUSION AND OUTLOOK

532 We have delved into the onset of freezing and  
 533 phase cross-over in 1D spin systems driven by a time-  
 534 periodic transverse field, contrasting the responses  
 535 in the Transverse Field Ising Model (TFIM) with that  
 536 of the long-range Lipkin-Meshkov-Glick Model (LMG).  
 537 The parametrization of DMBL is based on the Inverse  
 538 Participation Ratio (IPR) of the Floquet eigenstates.  
 539 Our investigations compared the IPRs from both mod-  
 540 els numerically, and found the emergence of thermal  
 541 behavior at low frequencies and freezing at high fre-

542 quencies for the LMG model, the latter a direct conse-  
 543 quence of the appearance of additional approximately  
 544 conserved quantities.

545 Long-range spins exhibit strong localization in spin-  
 546 coordinate space for the LMG model when the drive  
 547 frequency is  $\omega \gg J$ , where  $J$  represents the spin ex-  
 548 change energy. The localization of the LMG model  
 549 occurs at specific resonance points of the drive fre-  
 550 quency  $\omega$  and amplitude  $h$ , at  $J_0(4h/\omega) = 0$ ,  $\omega \gg J$ .  
 551 This is apparently similar to the phenomenon of Dy-  
 552 namical Freezing (DMF) in the Transverse Field Ising  
 553 Model (TFIM), where comparable localization at res-  
 554 onance points, determined by the roots of  $J_0(2h/\omega)$ ,  
 555 occurs due to the onset of an additional approximate  
 556 conservation in the transverse field itself. However,  
 557 a key difference is the thermal behaviour of the LMG  
 558 model at low frequencies. Plots of the IPR for a range  
 559 of frequencies along the resonance manifold exhibits  
 560 a smooth increase in IPR yielding a quantum phase-  
 561 crossover from a thermal phase governed by the Flo-  
 562 quet Eigenstate Thermalization Hypothesis (FETH) to  
 563 a Dynamically Many-Body localized phase (DMBL).  
 564 This crossover is absent in the TFIM, as can be readily  
 565 seen in the significant magnitude of the inverse par-  
 566 ticipation ratio (IPR) even at low frequencies. Thus,  
 567 the suppression of thermalization through Dynamical  
 568 Many Body Localization in long-range systems can be  
 569 controlled via Floquet engineering, even in clean sys-  
 570 tems without any disorder. Thus, periodically driven  
 571 long-range spin systems are an excellent tool for in-  
 572 vestigating disorder-free Many Body Localization, as  
 573 can be readily seen via the IPR of its Floquet modes.

574 There are several unexplored indicators of DMBL,  
 575 such as entanglement entropy and level statistics [10],  
 576 which we defer to future studies. In addition,  
 577 Halpern in 2019 proposed a quantum engine based  
 578 on MBL[11] which works between strong localized  
 579 and thermal phases of the system. In our proposed  
 580 LMG model, tuning the system parameters by bring-  
 581 ing them to the resonance points, then adiabatically  
 582 cycling the frequency from the thermal region to the  
 583 DMBL region, can achieve a similar engine without  
 584 going through a phase transition.

## A. Acknowledgements:

586 One of the authors, MR acknowledges The Univer-  
 587 sity of Burdwan for support via a state-funded fel-  
 588 lowship. AR acknowledges support from the Uni-  
 589 versity Grants Commission (UGC) of India, via BSR  
 590 Startup Grant No. F.30-425/2018(BSR), as well as  
 591 from the Science and Engineering Research Board  
 592 (SERB) Core Research Grant No. CRG/2018/004002.

- [1] S. Bordia Pranjal, Lüschen Henrik, *Nature Physics* **13**, 460 (2017).
- [2] S. Sahoo, I. Schneider, and S. Eggert, Periodically driven many-body systems: A floquet density matrix renormalization group study (2019), arXiv:1906.00004 [cond-mat.str-el].
- [3] A. Das, *Phys. Rev. B* **82**, 172402 (2010).
- [4] G. B. Mbeng, A. Russomanno, and G. E. Santoro, The quantum ising chain for beginners (2020), arXiv:2009.09208 [quant-ph].
- [5] H. S. Yamada and K. S. Ikeda, *Phys. Rev. E* **105**, 054201 (2022).
- [6] A. Roy and A. Das, *Phys. Rev. B* **91**, 121106 (2015).
- [7] H. Li, B. Shapiro, and T. Kottos, *Phys. Rev. B* **98**, 121101 (2018).
- [8] A. Eckardt and E. Anisimovas, *New Journal of Physics* **17**, 093039 (2015).
- [9] L. Zhang, V. Khemani, and D. A. Huse, *Phys. Rev. B* **94**, 224202 (2016).
- [10] V. Khemani, A. Lazarides, R. Moessner, and S. L. Sondhi, *Phys. Rev. Lett.* **116**, 250401 (2016).
- [11] N. Yunger Halpern, C. D. White, S. Gopalakrishnan, and G. Refael, *Phys. Rev. B* **99**, 024203 (2019).
- [12] T. Nag, S. Roy, A. Dutta, and D. Sen, *Phys. Rev. B* **89**, 165425 (2014).
- [13] G. Carleo, F. Becca, M. Schiró, and M. Fabrizio, *Scientific Reports* **2**, 243 (2012).
- [14] S. Aditya and D. Sen, Dynamical localization and slow thermalization in a class of disorder-free periodically driven one-dimensional interacting systems (2023), arXiv:2305.06056 [cond-mat.stat-mech].
- [15] M. Schiulaz, A. Silva, and M. Müller, *Phys. Rev. B* **91**, 184202 (2015).
- [16] T. Grover and M. P. A. Fisher, **2014**, P10010.
- [17] Z. Papić, E. M. Stoudenmire, and D. A. Abanin, *Annals of Physics* **362**, 714 (2015).
- [18] A. Smith, J. Knolle, D. L. Kovrizhin, and R. Moessner, *Phys. Rev. Lett.* **118**, 266601 (2017).
- [19] O. Hart, S. Gopalakrishnan, and C. Castelnovo, *Phys. Rev. Lett.* **126**, 227202 (2021).
- [20] H. Lipkin, N. Meshkov, and A. Glick, *Nuclear Physics* **62**, 188 (1965).
- [21] N. Meshkov, A. Glick, and H. Lipkin, *Nuclear Physics* **62**, 199 (1965).
- [22] A. Glick, H. Lipkin, and N. Meshkov, *Nuclear Physics* **62**, 211 (1965).
- [23] P. Ribeiro, J. Vidal, and R. Mosseri, *Phys. Rev. E* **78**, 021106 (2008).
- [24] N. Debergh and F. Stancu, *Journal of Physics A: Mathematical and General* **34**, 3265 (2001).
- [25] P. Titum and M. F. Maghrebi, *Phys. Rev. Lett.* **125**, 040602 (2020).
- [26] A. Campa, T. Dauxois, and S. Ruffo, *Physics Reports* **480**, 57 (2009).
- [27] E. R. S. Eisele, *Theodor, Journal of Statistical Physics*, 161 (1988).
- [28] A. Canning, *Physica A: Statistical Mechanics and its Applications* **185**, 254 (1992).
- [29] D. Vu, K. Huang, X. Li, and S. Das Sarma, *Phys. Rev. Lett.* **128**, 146601 (2022).
- [30] G. Misguich, V. Pasquier, and J.-M. Luck, *Phys. Rev. B* **94**, 155110 (2016).
- [31] M. Calixto and E. Romera, *Journal of Statistical Mechanics: Theory and Experiment* **2015**, P06029 (2015).
- [32] K. Fujii, *Journal of Modern Physics* **8**, 2042 (2017).
- [33] D. A. Abanin, E. Altman, I. Bloch, and M. Serbyn, *Rev. Mod. Phys.* **91**, 021001 (2019).
- [34] M. Srednicki, *Phys. Rev. E* **50**, 888 (1994).
- [35] M. Srednicki, *Journal of Physics A: Mathematical and General* **32**, 1163 (1999).
- [36] M. Holthaus, *Journal of Physics B: Atomic, Molecular and Optical Physics* **49**, 013001 (2015).
- [37] M. Vogl, M. Rodriguez-Vega, and G. A. Fiete, *Phys. Rev. B* **101**, 024303 (2020).
- [38] M. Bukov, L. D'Alessio, and A. Polkovnikov, *Advances in Physics* **64**, 139 (2015).
- [39] L. D'Alessio and M. Rigol, *Phys. Rev. X* **4**, 041048 (2014).
- [40] R. Yousefjani, S. Bose, and A. Bayat, *Phys. Rev. Res.* **5**, 013094 (2023).
- [41] P. Sierant, M. Lewenstein, A. Scardicchio, and J. Zakrzewski, *Phys. Rev. B* **107**, 115132 (2023).
- [42] R. Yousefjani, S. Bose, and A. Bayat, *Phys. Rev. Res.* **5**, 013094 (2023).
- [43] F. Alet and N. Laflorencie, *Comptes Rendus Physique* **19**, 498 (2018).
- [44] S. J. Garratt and S. Roy, *Phys. Rev. B* **106**, 054309 (2022).
- [45] R. B. Stinchcombe, *Journal of Physics C: Solid State Physics* **6**, 2459 (1973).
- [46] F. E. H. George Arfken, Hans Weber, *Mathematical Methods for Physicists*, 7th ed. (Academic Press).
- [47] S. Mukherjee, A. Spracklen, D. Choudhury, N. Goldman, P. Öhberg, E. Andersson, and R. R. Thomson, *New Journal of Physics* **17**, 115002 (2015).
- [48] S.-H. Lin, B. Sbierski, F. Dorfner, C. Karrasch, and F. Heidrich-Meisner, *SciPost Phys.* **4**, 002 (2018).
- [49] N. C. Murphy, R. Wortis, and W. A. Atkinson, *Phys. Rev. B* **83**, 184206 (2011).
- [50] E. J. Torres-Herrera, I. Vallejo-Fabila, A. J. Martínez-Mendoza, and L. F. Santos, *Phys. Rev. E* **102**, 062126 (2020).
- [51] N. Trivedi and D. Heidarian, *Progress of Theoretical Physics Supplement* **160**, 296 (2005).
- [52] G. Misguich, V. Pasquier, and J.-M. Luck, *Phys. Rev. B* **94**, 155110 (2016).
- [53] A. Russomanno, R. Fazio, and G. E. Santoro, *Europhysics Letters* **110**, 37005 (2015).
- [54] N. Defenu, T. Enss, M. Kastner, and G. Morigi, *Phys. Rev. Lett.* **121**, 240403 (2018).
- [55] T. Mori, *Journal of Physics A: Mathematical and Theoretical* **52**, 054001 (2019).
- [56] J. Johansson, P. Nation, and F. Nori, *Computer Physics Communications* **184**, 1234.
- [57] B. Sciolla and G. Biroli, *Phys. Rev. Lett.* **105**, 220401 (2010).

- <sup>709</sup> [58] R. A. Kidd, M. K. Olsen, and J. F. Corney, Phys. Rev. A <sup>729</sup> [66] B. Marcos, A. Gabrielli, and M. Joyce, Open Physics **10**,  
<sup>710</sup> **100**, 013625 (2019). <sup>730</sup> 676.
- <sup>711</sup> [59] A. Bäcker, S. Fürstberger, and R. Schubert, Phys. Rev. <sup>731</sup> [67] A. Haldar and A. Das, Annalen der Physik **529**,  
<sup>712</sup> E **70**, 036204 (2004). <sup>732</sup> 1600333.
- <sup>713</sup> [60] S. Sachdev, *Quantum Phase Transitions*, 2nd ed. (Cam- <sup>733</sup> [68] J. M. Deutsch, Phys. Rev. A **43**, 2046 ().  
<sup>714</sup> bridge University Press, Cambridge, 2011). <sup>734</sup> [69] E. W. Hobson, On the Second Mean-Value Theorem of  
<sup>715</sup> [61] P. Reimann, Journal of Statistical Mechanics: Theory <sup>735</sup> the Integral Calculus (1909).  
<sup>716</sup> and Experiment **2021**, 103106 (2021).
- <sup>717</sup> [62] When frozen,  $|\psi(t)\rangle \approx |s_N\rangle$ . From eqn 17,  $\langle \hat{H}_{0,1} \rangle$  are <sup>736</sup> [70] M. Rigol and M. Srednicki, Physical Review Letters  
<sup>718</sup> both approximately constant. Averaging the square of <sup>737</sup> **108**, 10.1103/physrevlett.108.110601 (2012).  
<sup>719</sup>  $\langle \hat{H}(t) \rangle$  over long times  $\tau \gg T$  yields a result that goes <sup>738</sup> [71] J. M. Deutsch, IOP Publishing Ltd **81**, 296 ().  
<sup>720</sup> as  $h^2 + \delta$ , where  $\delta \sim h_0 \ll 1$ . Thus, the standard devia- <sup>739</sup> [72] R. Nandkishore and D. A. Huse, Annual Review of Condensed Matter Physics **6**, 15 (2015),  
<sup>721</sup> tion in time will go as  $\sim h \sim \omega$ , since  $\eta = 4h/\omega$  is kept <sup>740</sup> <https://doi.org/10.1146/annurev-conmatphys-031214-014726>.
- <sup>722</sup> fixed. <sup>741</sup> [73] L. D'Alessio and A. Polkovnikov, **333**, 19.
- <sup>723</sup> [63] L. Reichl, *The Transition to Chaos: Conservative Clas- <sup>742</sup> [74] S. Notarnicola, F. Iemini, D. Rossini, R. Fazio, A. Silva,  
<sup>724</sup> sical and Quantum Systems*, Fundamental Theories of <sup>743</sup> and A. Russomanno, Phys. Rev. E **97**, 022202 (2018).  
<sup>725</sup> Physics, Vol. 200 (Springer International Publishing). <sup>744</sup> [75] A. Lazarides, A. Das, and R. Moessner, Phys. Rev. Lett.  
<sup>726</sup> [64] N. Srivatsa, R. Moessner, and A. E. Nielsen, Phys. Rev. <sup>745</sup> **115**, 030402 (2015).
- <sup>727</sup> Lett. **125**, 240401.
- <sup>728</sup> [65] Quantum ising phase transition.